Length scale dependent deformation in natural rubber

Gurudutt Chandrashekar, Farid Alisafaei, Chung-Souk Han

Department of Mechanical Engineering, University of Wyoming, 1000 E. University Ave, Laramie Wyoming 82071
Correspondence to: G. Chandrashekar (E-mail: gchandra@uwyo.edu)

ABSTRACT: Strong length scale dependent deformation has been previously observed in the elastomer polydimethylsiloxane by indentation type experiments at micro- to nanometer length scales with a sharp conical tip. To examine if other nonsilicone based elastomers exhibit similar length scale dependent deformation behavior, natural rubber has been chosen in this study. Performing indentation type tests with a nanoindentation system, the universal hardness and the elastic modulus are determined at different probing depths ranging from about 90 to 5 μm to characterize length scale dependent deformation behavior in natural rubber. The testing with a Berkovich tip resulted in an amazing increase in the universal hardness with decreasing probing depth indicating that the deformation mechanisms at the micrometer length scales are significantly different as compared to those at the macroscopic length scales. The observed length scale dependent deformation is associated with an increase in rotation gradients with decreasing probing depth. © 2015 Wiley Periodicals, Inc. J. Appl. Polym. Sci. **2015**, *132*, 42683.

INTRODUCTION

Nanoindentation techniques are widely applied to determine the material properties of polymers at micro and nanometer length scales.[1–6] The deformation mechanisms at the micrometer length scale and below can be significantly different when compared to the macroscopic length scale. The nanoindentation techniques have been applied by various researchers to study the indentation depth dependent deformation in metals[7] and polymers.[8–21] However, unlike metals, where length scale dependent deformation in the considered length scale range is usually attributed to geometrically necessary dislocations and corresponding nonuniform plastic deformation,[7] an understanding of the origin of length scale dependent deformation in polymers is far from clear. In contrast to the size dependent mechanism observed in metals, micro-beam bending experiments on epoxy by Lam *et al.*[22] revealed the existence of size effects in elastic deformation of polymers exemplifying the different characteristics of length scale dependent deformation in polymers compared to metals.

Indentation experiments on PDMS[18,19,23] and other silicone based elastomers[12,24] revealed astonishing indentation size effects, which give rise to the question if such significant size effects can be observed in other elastomers as well. In the present work, the size dependent deformation of natural rubber is investigated at micrometer length scale range (4.7–90 μm) with a pyramidal Berkovich tip as well as a spherical tip where the

hardness, the dissipation and other parameters are examined to characterize the length scale dependent deformation in natural rubber.

Natural rubber is widely used commercially for various applications. For instance, natural rubber is used in the tire industry where a typical tire can be considered to be composed of layers of macroscopic composites with long reinforcing fibers or wires surrounded by rubber material.[25] Other applications where natural rubber is applied in small length scales include polymer composites,[26,27] foams,[28] surfaces,[29] and sealants.[30]

EXPERIMENTAL

Material

A natural rubber, NR (catalog nos. 8633K52) sample was obtained from McMaster Carr (Los Angeles, CA) and the sample was tested as received. Since natural rubber is constituted of natural components, it exhibits significant inhomogeneity which is evident from Figure 1 where a surface photograph of the natural rubber sample is shown.

Indentation Testing

The indentation tests were conducted using an Agilent Nanoindenter G200 system (Agilent Technologies, Oak Ridge, TN) equipped with XP and DCM indenter heads. The indentation tests to determine the hardness were carried out with the XP head using a Berkovich tip with a nominal curvature radius of 20 nm (according to the manufacturer's specifications). The
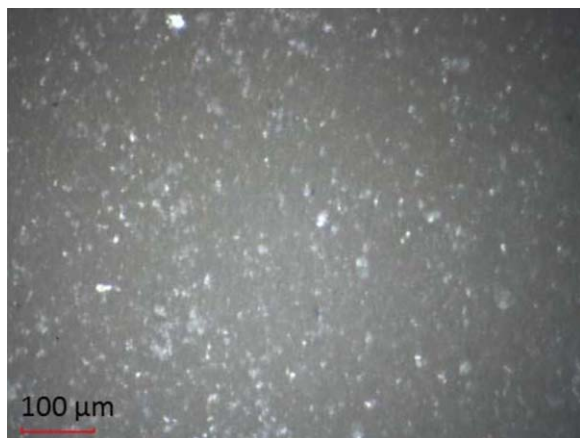
Figure 1. Natural rubber sample depicting inhomogeneity at the surface. [Color figure can be viewed in the online issue, which is available at wileyonlinelibrary.com.]

Figure 2. Probing depth h measured at the maximum applied force F_{max}. [Color figure can be viewed in the online issue, which is available at wileyonlinelibrary.com.]

elastic modulus was determined with the XP head using a spherical tip with a curvature radius of 250 μm. All tests were performed at an ambient temperature of about 23°C with loading and unloading times of 20 s (without holding time) where the load was applied linearly in time. The maximum applied force F_{max} ranged between 0.36 and 29.88 mN with the corresponding probing depth h between 4.7 and 90 μm. A surface detection stiffness criterion (detailed in the next subsection) of 50 N/m was applied for all the indentation tests.

To investigate the effect of loading time on the indentation size effects, indentation tests were also conducted for a loading time of 70 s. Figure 2 illustrates h-F_{max} curve for 20 and 70 s loading times obtained over the entire range of probing depths. As depicted in Figure 2, there is hardly any variation in the probing depth h for a given F_{max} at loading times of 20 and 70 s. Each data point in Figure 2 represents the mean of probing depths obtained at a given F_{max} with an error bar being the standard deviation of the mean divided by the square root of two (number of tests).

The experimentally determined load-displacement data is utilized to calculate the universal hardness based on ISO 14577-1[31] as:

$$H_U = \frac{F_{max}}{Ch^2} \qquad (1)$$

where C is a constant equal to 26.43 for a Berkovich tip and the term Ch^2 in eq. (1) represents the nominal surface area of the indenter tip penetrating beyond the initial point of contact under the applied maximum force F_{max}. Unlike the indentation hardness,[32] which has been mainly developed for materials subjected to plastic deformation, the universal hardness is applicable to all materials since it incorporates both elastic and plastic deformations.[14,31]
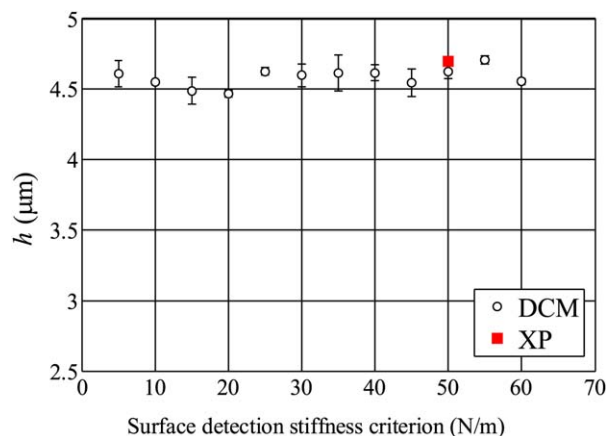
Surface Detection Criterion

Accurate detection of the surface of soft materials can pose significant challenges in nanoindentation testing.[33,34] For soft materials, an underestimation of the contact area leads to an
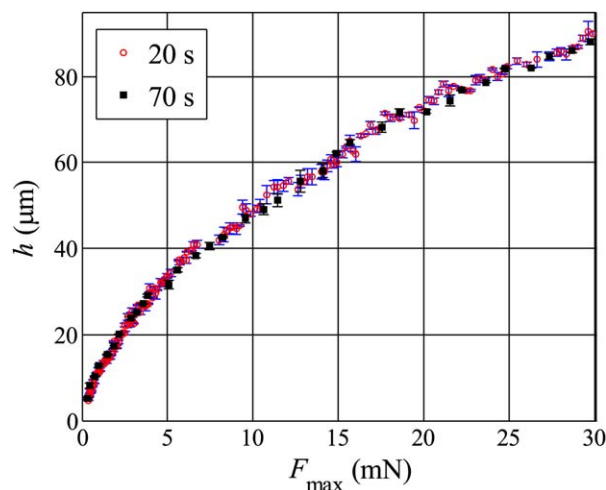
overestimation of the determined properties.[33] The surface of the sample is detected when the stiffness of the sample exceeds the prescribed surface detection stiffness criterion, K_{tol}^S. The nanoindenter system (identical to the one use by Alisafaei et al.[19]) is equipped with a highly sensitive dynamic contact module (DCM) head and a comparatively less sensitive XP head. Unlike the DCM head, the resonant frequency of the XP head is quite low (13 Hz) and it can quite often be susceptible to environmental noise at lower K_{tol}^S.

While the DCM head is better insulated from vibrations and can be applied with lower K_{tol}^S values,[19] it has a limitation in applicable probing depths which should not exceed 5 μm. To obtain the appropriate K_{tol}^S for the XP head, the selected K_{tol}^S is validated with the DCM head, which was found to be able to accurately detect the surface of PDMS over a range of K_{tol}^S.[19] As presented in Figure 3, the probing depth at a load of 0.36 mN (lowest load) using a K_{tol}^S of 50 N/m with the XP head and a Berkovich tip, was found to match the probing depth obtained

Figure 3. Probing depth versus surface detection stiffness criterion for F_{max} of 0.36 mN with a loading time of 20 s. [Color figure can be viewed in the online issue, which is available at wileyonlinelibrary.com.]
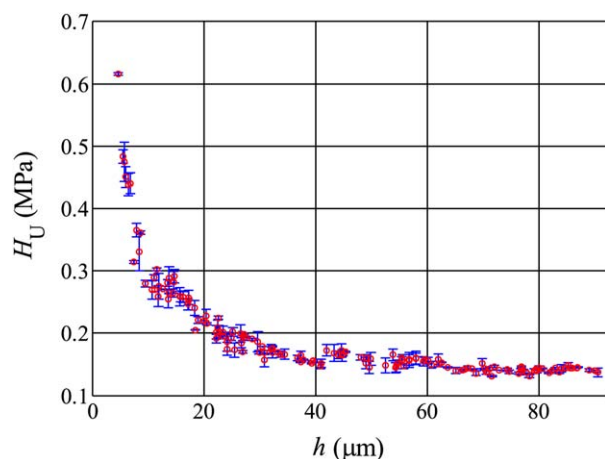
Figure 4. Universal hardness H_U versus h for a loading time of 20 s. [Color figure can be viewed in the online issue, which is available at wileyonlinelibrary.com.]

Figure 5. Schematic representation of loading-unloading curve depicting the elastic and inelastic work. [Color figure can be viewed in the online issue, which is available at wileyonlinelibrary.com.]

with the DCM head over a range of surface detection criteria (5–60 N/m) illustrating the appropriateness of 50 N/m as K_{tol}^S.

EXPERIMENTAL RESULTS

Hardness

The universal hardness at probing depth h ranging from 4.7 to 90 μm for a loading time of 20 s is depicted in Figure 4. It can be observed that there is a significant increase in the universal hardness H_U (0.13–0.61 MPa) with decreasing probing depth (90–4.7 μm). Since there was hardly any change in the probing depth for a given F_{max} with the 70 s loading time (in comparison to the 20 s loading time as shown in Figure 2), rate effects appear to be negligible (at least for loading times in the same order of magnitude) for the investigated length scale range.

Dissipation and Indentation Work

The dissipation of the deformation work over the range of probing depths can be used to understand the probing depth dependent behavior of natural rubber. A schematic depiction of the total work W_I is presented in Figure 5 where the elastic component W_I^e and inelastic component W_I^{ine} can be clearly distinguished. Accordingly, the total work W_I can be represented as:

$$W_I = W_I^e + W_I^{ine} \tag{2}$$

To relate the dissipation to the total deformation work in natural rubber at different probing depths h, a parameter η^e is introduced. This parameter η^e is defined as:

$$\eta^e = \frac{W_I^e}{W_I} \tag{3}$$

and a decrease in the parameter η^e indicates an increase in dissipation. Figure 6 illustrates η^e versus h for 20 s loading time where there is significant increase in dissipation with decreasing probing depth due to the decrease in elastic component W_I^e. The load-displacement curves at the minimum and maximum applied loads (0.36 and 29.88 mN) for a loading time of 20 s are presented in Figure 7, where the decrease in the elastic component of work with decreasing depth can be clearly seen. Similar trend
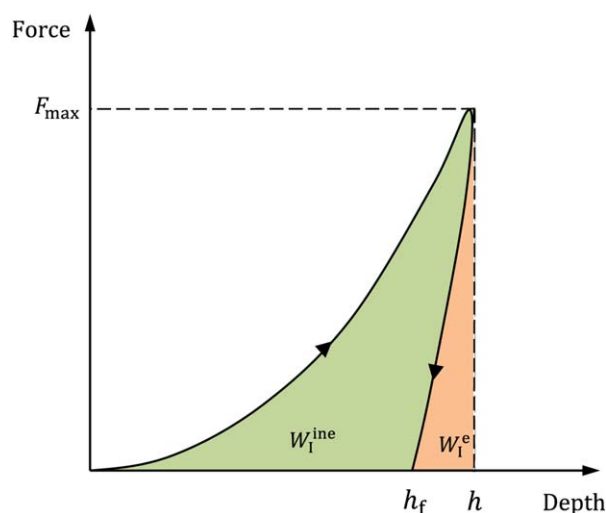
was also observed for various other polymers where a plasticity index was used to characterize the relative elastic/plastic behavior of polymer materials.[17] The change in the slope of η^e, which is observed at $\sim h = 18$ μm (denoted in Figure 6 as h_d) may be related to the effect of surface roughness becoming important below this probing depth, which will be discussed later.

Elastic Modulus

To quantify the variation in the homogeneity of the natural rubber sample through thickness, the elastic modulus of natural rubber is determined at different probing depths ranging from about 90 to 4.7 μm. The elastic modulus is determined using the Hertzian contact theory[35] by applying a spherical tip with a curvature radius of 250 μm, and also with Sneddon's theory[36] using a Berkovich tip. The Hertzian contact theory considers the elastic contact of a sphere with a half space and the Sneddon's theory is applicable for frictionless indentation of elastic materials utilizing a conical tip.
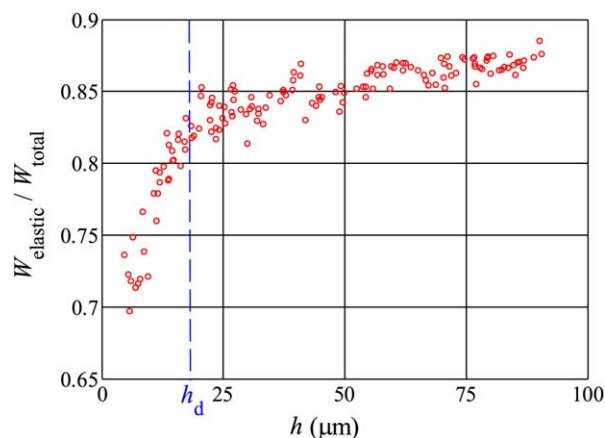
Figure 6. Ratio of elastic work to total deformation work versus h. [Color figure can be viewed in the online issue, which is available at wileyonlinelibrary.com.]
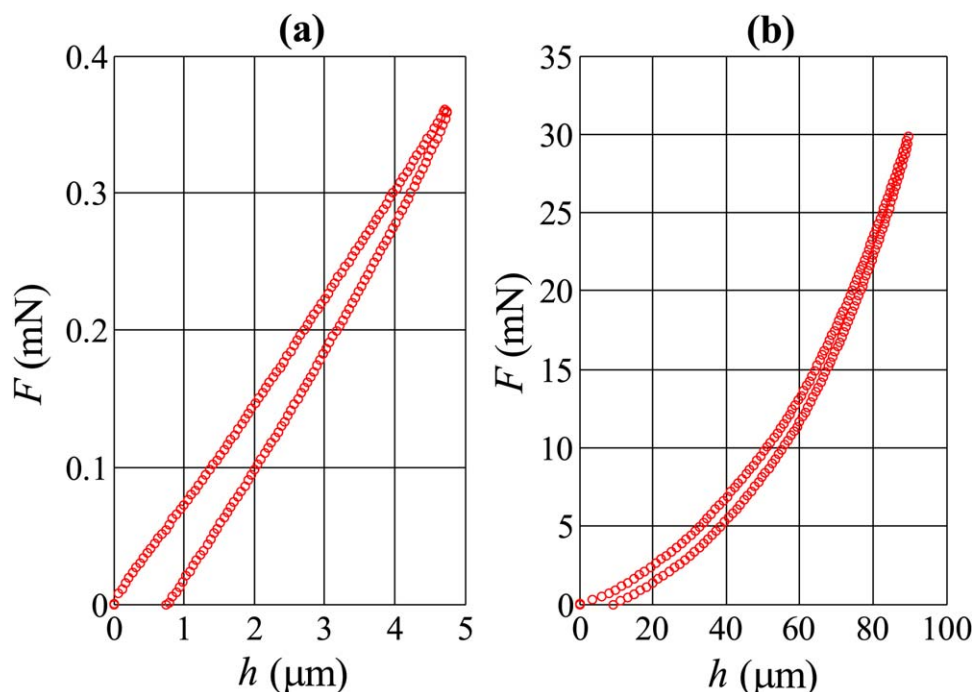
Figure 7. Typical load-displacement curves at (a) minimum applied load of 0.36 mN and (b) maximum applied load of 29.88 mN. [Color figure can be viewed in the online issue, which is available at wileyonlinelibrary.com.]

The Hertzian contact theory (assuming linear elasticity and a small ratio of the contact area to the curvature radius of the spherical tip) gives the following relation:

$$F = \frac{4}{3}\left(\frac{h}{R}\right)^{\frac{3}{2}} R^2 E_r \qquad (4)$$

where F is the applied force, R is the radius of the sphere, h is the probing depth and E_r is the reduced elastic modulus, which is related to the elastic modulus of the polymer, E_p, via:

$$\frac{1}{E_r} = \frac{1-v_p^2}{E_p} + \frac{1-v_i^2}{E_i} \qquad (5)$$

where E_i and v_i are respectively the elastic modulus and Poisson's ratio of the indenter tip and v_p is the Poisson's ratio of the polymer. Since, $E_i >> E_p$, the elastic modulus of the polymer is obtained as:

$$E_p^{\text{Hertz}} = (1-v_p^2) E_r \qquad (6)$$

The Sneddon's theory for frictionless contact is given by:

$$F = \frac{2E_p \tan\alpha}{\pi(1-v_p^2)} h^2 \qquad (7)$$

where E_p is the modulus of the polymer, $\alpha = 70.3°$ the half angle defining a cone equivalent to a Berkovich tip and v_p the Poisson's ratio of the polymer. Figure 8 depicts the elastic modulus of natural rubber over the range of probing depths utilizing the Berkovich tip and the spherical tip.

As illustrated in Figure 8, the application of Hertz theory (with spherical tip) results in a negligible variation in the elastic modulus with varying probing depth while in contrast, the application of Sneddon's theory (with Berkovich tip) gives rise to the

increase of elastic modulus with decreasing depth. This observed discrepancy in the results obtained by applying the two tips with different geometries is discussed below based on a rotation gradient based model.

EXPERIMENTAL UNCERTAINTIES

Tip Bluntness

To determine the influence of the tip bluntness on the experimental results, the Berkovich tip is modeled by a cone smoothly fitted with a spherical cap of a certain curvature radius.[20] Figure 9 depicts the projected contact area A_c obtained from
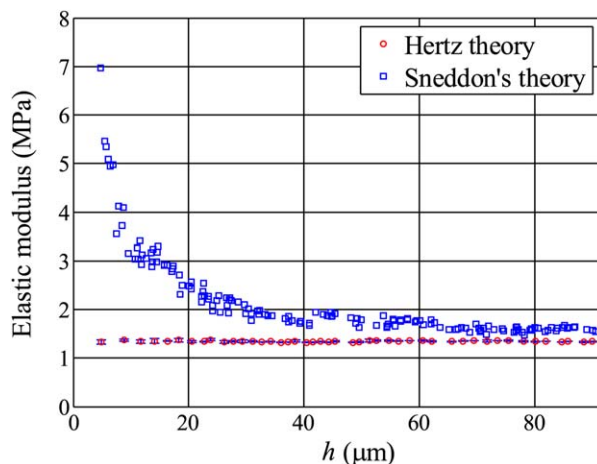
Figure 8. Elastic modulus of natural rubber with respect to probing depth h using spherical (Hertz theory) and Berkovich (Sneddon's theory) indenter tips. [Color figure can be viewed in the online issue, which is available at wileyonlinelibrary.com.]
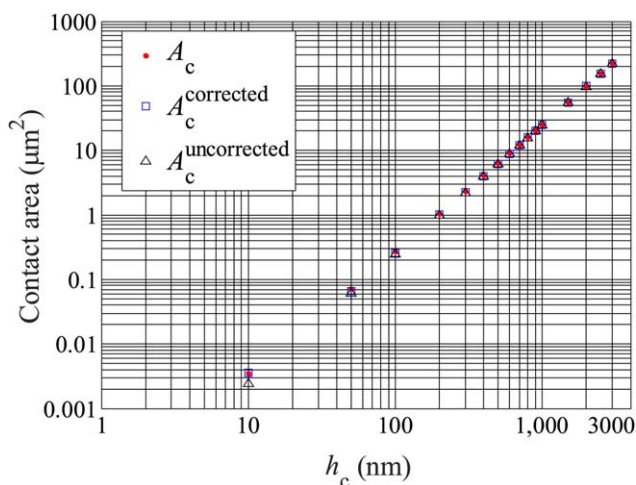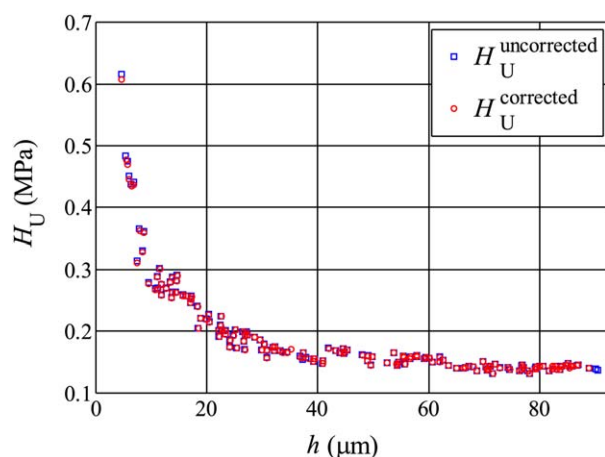
Figure 9. Different contact areas (A_c, $A_c^{corrected}$, $A_c^{uncorrected}$) versus contact depth h_c for fused silica. [Color figure can be viewed in the online issue, which is available at wileyonlinelibrary.com.]

Figure 11. Raw displacement versus raw load for 20 s loading time. [Color figure can be viewed in the online issue, which is available at wileyonlinelibrary.com.]
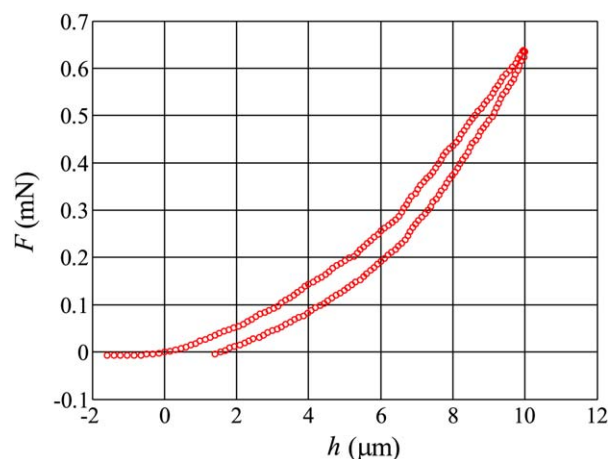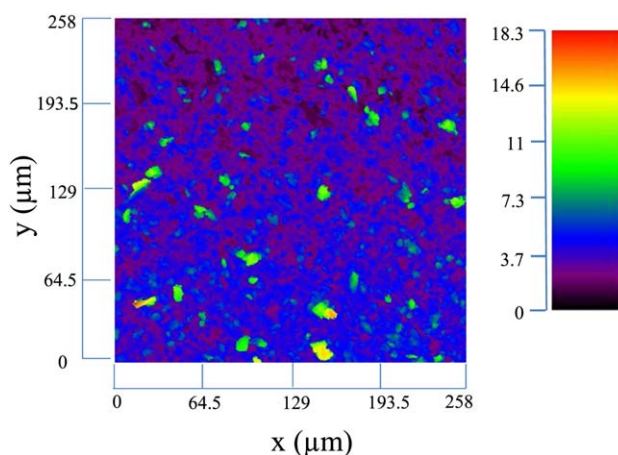
nanoindentations on fused silica, the projected contact area $A_c^{uncorrected}$ of an ideal Berkovich tip and the projected contact area $A_c^{corrected}$ obtained by fitting the projected contact area A_c with the contact area of a rounded tip.[20] The calculated tip curvature radius obtained from the curve fitting was found to be 32.17 nm, which would result in a new nominal surface area of the blunted indenter tip. It can be seen in Figure 10 that there is a negligible variation in the universal hardness values obtained from the nominal surface area of the blunted tip and the nominal surface area of an ideally sharp Berkovich tip indicating negligible influence of the tip bluntness on the indentation size effects observed in the present investigation.

Influence of Adhesion on the Indentation Size Effects

Adhesive forces can be quite significant in the nanoindentation of soft polymeric materials, especially at lower probing depths.[37] The soft polymers, especially tacky polymers could get attracted to the tip resulting in a negative load at the beginning of the

indentation procedure. If adhesive forces are significant, the initial contact point between the tip and the material could be different when compared to the initial contact point detected by the automated indentation system. The raw load- raw displacement data at a load of 0.63 mN has been presented in Figure 11, where negligible adhesive forces can be observed.

Surface Roughness of Natural Rubber

To determine the influence of surface roughness on the observed indentation size effects, three different areas of the sample with dimensions of 258 μm by 258 μm were investigated under an optical profilometer (LEXT 3D measuring microscope OLS 4000-OLYMPUS). The profile of the surface roughness of one such area on the sample is depicted in Figure 12. The average of the surface roughness parameter S_a (arithmetic mean of the absolute of the ordinate values within a definition area) of three sample areas, in accordance with ISO 25178-2:2012, was found to be 858 nm. The mean of S_z (sum of the maximum peak height value and the maximum pit height value within a

Figure 10. Effect of tip roundness on H_U for the natural rubber sample. [Color figure can be viewed in the online issue, which is available at wileyonlinelibrary.com.]

Figure 12. Surface profile of the natural rubber sample. [Color figure can be viewed in the online issue, which is available at wileyonlinelibrary.com.]
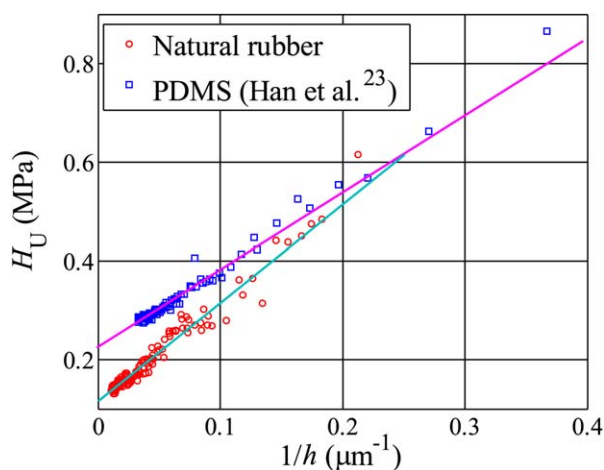
Figure 13. Universal hardness H_U versus inverse of probing depth $1/h$ for the natural rubber sample and a PDMS sample from Han *et al.*[23] (with 20 s loading time). [Color figure can be viewed in the online issue, which is available at wileyonlinelibrary.com.]

definition area) of three sample areas, in accordance with ISO 25178-2:2012, was found to be 18.52 μm, which corresponds to the depth (denoted in Figure 6 as h_d) where the change in the slope in dissipation is observed. It is known that rough indented surfaces increase the dissipation of indentation work, resulting in an increase in indentation size effects.[15,16] This is evident from the fact that as the probing depth is decreased from 18 to 4.7 μm, there is a 2.5-fold increase in the universal hardness in contrast to the 1.85-fold increase in the hardness as the indentation depth is reduced from 90 to 18 μm. Although the surface roughness has a significant influence on the observed indentation size effects, it cannot be viewed as the only source of size effects as significant increase in the hardness was observed at higher probing depths where surface roughness does not have an influence on the indentation results.

DISCUSSION

Influence of Rotation Gradients on the Determination of Universal Hardness in Natural Rubber

On the basis of a previously developed model,[38,39] the observed increase in the universal hardness of natural rubber with decreasing depth is believed to be a result of increase in rotation gradients with decreasing depth. The deformation work represented by eq. (2) is augmented by a nonlocal component ΔW^F (containing rotations gradients), which is influenced by the bending rigidity of the polymer chain,[13] molecular weight,[11] and crosslink density.[10] The deformation work W_I following the augmentation of ΔW^F is given by:

$$W_I = W_I^e + W_I^{ine} + \Delta W_I^F \qquad (8)$$

The increase in rotation gradients with decreasing probing depth gives rise to a corresponding increase in the value of ΔW_I^F resulting in the increase in hardness values.[38,39] In contrast to a Berkovich tip, a spherical tip would cause negligible changes in the rotation gradients with changing depth.[40,41] Therefore, using a spherical tip would not cause the depth dependence in hardness.

Influence of Rotation Gradients on the Determination of Elastic Modulus of Natural Rubber

The observed discrepancy in the elastic modulus results (Figure 8) obtained by using the spherical tip (applying Hertz theory[35]) and the Berkovich tip (applying Sneddon's theory[36]) can be attributed to the influence of rotation gradients with varying probing depth. The application of a Berkovich tip results in the increase of rotation gradients with decreasing probing depth while applying a spherical tip causes negligible influence on the rotation gradients with varying depth.[40,41] As the magnitude of the rotation gradients becomes negligible at higher probing depths, the Hertzian contact theory and the Sneddon's theory would yield identical results as shown in Figure 8. As the results obtained by applying a spherical tip are not influenced by the rotation gradients at lower probing depths, the elastic modulus determined by the spherical tip should be considered as the true modulus of the natural rubber sample. The negligible variation in the elastic modulus with varying depth obtained by applying a spherical tip also invalidates surface inhomogeneity as one of the causes of indentation size effects.

Influence of Stress Relaxation on the Length Scale Dependent Deformation in Natural Rubber

The influence of stress relaxation on the length scale dependent deformation in natural rubber was found be to be negligible for the considered loading times of 20 and 70 s. However, as polymers are known to be rate dependent, with increases in loading time by multiple orders of magnitude, the influence of the stress relaxation may become more pronounced due to the rearrangement and relaxation of polymer chains.

Interestingly, with the change in loading time, the influence of stress relaxation on the length scale dependent deformation in PDMS[19] was evident at indentation depths below 1 μm. Because of the considerable surface roughness of the natural rubber sample; the minimum probing depth was curtailed to 4.7 μm, which would restrict the understanding of the stress relaxation behavior and the resulting length scale dependent deformation at lower probing depths.

Theoretical Hardness Model

The experimental results are analyzed utilizing a depth dependent hardness model suggested by Han *et al.*[39] where previously a good agreement was found with PDMS,[19] filled Silicone rubber[12] and epoxy.[20] The depth dependent hardness model is given by:

$$H = H_0 \left(1 + \frac{C_\ell}{h}\right) \qquad (9)$$

where H_0 is the macroscopic hardness of the material and C_ℓ is the length scale parameter of the material.[39] Figure 13 depicts

Table I. Macroscopic Hardness H_0 and the Length Scale Parameter C_ℓ for Natural Rubber and PDMS

Elastomer	H_0 (MPa)	C_ℓ (μm)
Natural rubber	0.1136	18.09
PDMS	0.2191	7.694

the plot of the inverse of probing depth versus the hardness for natural rubber and PDMS[23] (extracted data) where C_ℓ and H_0 have been determined by fitting eq. (9) to the experimental data and are given in Table I for both the elastomers.

CONCLUSIONS

Indentation type testing was conducted on natural rubber at probing depths ranging from 4.7 to 90 μm. The amazing length scale effects observed in the investigated probing range were analyzed using a depth dependent hardness model. It was also observed that loading time had little influence on the hardness for the investigated length scale range. The dissipation of deformation work of natural rubber was depicted over the range of probing depths and a considerable increase in dissipation was observed with decreasing probing depth. A comparative study was made on the influence of different tips on the determination of elastic modulus of natural rubber proving the influence of rotation gradients on the calculated elastic modulus results. The highly elastic polymers such as natural rubber and PDMS exhibit enormous increases in hardness with decrease in depth, which is in contrast to the behavior observed in glassy polymers such as epoxy.[20]

ACKNOWLEDGMENTS

REFERENCES

1. Rianasari, I.; Weston, J.; Rowshan, R.; Blanton, T.; Khapli, S.; Jagannathan, R. *J. Appl. Polym. Sci.* **2015**, *132*, 41360.

2. Iqbal, T.; Briscoe, B. J.; Yasin, S.; Luckham, P. F. *J. Appl. Polym. Sci.* **2013**, *130*, 4401.

3. Mencík, J.; He, L. H.; Nemecek, J. *Polym. Test.* **2011**, *30*, 101.

4. VanLandingham, M. R.; Chang, N. K.; Drzal, P. L.; White, C. C.; Chang, S. H. *J. Polym. Sci.* **2005**, *43*, 1794.

5. Maxwell, A. S.; Monclus, M. A.; Jennett, N. M.; Dean, G. *Polym. Test.* **2011**, *30*, 366.

6. Tweedie, C. A.; Constantinides, G.; Lehman, K. E.; Brill, D. J.; Blackman, G. S.; Vliet, K. J. V. *Adv. Mater.* **2007**, *19*, 2540.

7. Nix, W. D.; Gao, H. *J. Mech. Phys. Solids* **1998**, *46*, 411.

8. Lam, D. C. C.; Chong, A. C. M. *J. Mater. Res.* **1999**, *14*, 3784.

9. Chong, A. C. M.; Lam, D. C. C. *J. Mater. Res.* **1999**, *14*, 4103.

10. Lam, D. C. C.; Chong, A. C. M. *Mater. Sci. Eng. A* **2000**, *281*, 156.

11. Tjernlund, J. A.; Gamstedt, E. K.; Xu, Z. H. *Polym. Eng. Sci.* **2004**, *44*, 1987.

12. Tatiraju, R. V. S.; Han, C.-S. *J. Mech. Mater. Struct.* **2010**, *5*, 277.

13. Han, C.-S. *Mater. Sci. Eng. A* **2010**, *527*, 619.

14. Lim, Y. Y.; Chaudhri, M. M. *Mech. Mater.* **2006**, *38*, 1213.

15. Zhang, T. Y.; Xu, W. H. *J. Mater. Res.* **2002**, *17*, 1715.

16. Zhang, T. Y.; Xu, W. H.; Zhao, M. H. *Acta Mater.* **2004**, *52*, 57.

17. Briscoe, B. J.; Fiori, L.; Pelillo, E. *J. Phys. D* **1998**, *31*, 2395.

18. Charitidis, C. *Ind. Eng. Chem. Res.* **2011**, *50*, 565.

19. Alisafaei, F.; Han, C.-S.; Sanei, S. H. R. *Polym. Test.* **2013**, *32*, 1220.

20. Alisafaei, F.; Han, C.-S.; Lakhera., N. *Polym. Test.* **2014**, *40*, 70.

21. Wrucke, A. J.; Han, C.-S.; Majumdar., P. *J. Appl. Polym. Sci.* **2013**, *128*, 258.

22. Lam, D. C. C.; Yang, F.; Chong, A. C. M.; Wang, J.; Tong, P. *J. Mech. Phys. Sol.* **2003**, *51*, 1477.

23. Han, C.-S.; Sanei, S. H. R.; Alisafaei, F. *J. Polym. Eng.* to appear, DOI: 10.1515/polyeng-2015-0030.

24. Xu, W.-H.; Xiao, Z.-Y.; Zhang, T.-Y. *Mater. Lett.* **2005**, *59*, 2153.

25. Hirata, Y.; Kondo, H.; Ozawa, Y. Chemistry, Manufacture and Applications of Natural Rubber; Kohjiya, S.; Ikeda, Y., Eds.; Woodhead: Kidlington, **2014**; Chapter 12, p 326.

26. Wu, L.; Qu, P.; Zhou, R.; Wang, B.; Liao, S. *High. Perform. Polym.* **2015**, *4*, 486.

27. Yao, H.; Weng, G.; Liu, Y.; Fu, K.; Chang, A.; Chen, Z.-R. *J. Appl. Polym. Sci.* **2015**, *132*, 41980.

28. Tangboriboon, N.; Samattai, S.; Kamonsawas, J.; Sirivat, A. *Mater. Manufac. Proc.* **2015**, *30*, 595.

29. Manhart, J.; Lenko, D.; Muehlbacher, I.; Hausberger, A.; Schaller, R.; Holzner, A.; Kern, W.; Schloegl, S. *Eur. Polym. J.* **2015**, *66*, 236.

30. Wang, L.; Xu, J. (Qingdao Changanda Pharm Co.). CN Pat. 104371590-A, **2015**.

31. ISO 14577-1; Metallic Materials—Instrumented Indentation Test for Hardness and Materials Parameters—Part 1: Test Method; International Organization for Standardization: Geneva, **2002**.

32. Oliver, W. C.; Pharr, G. M. *J. Mater. Res.* **1992**, *7*, 1564.

33. Kaufman, J. D.; Klapperich, C. M. *J. Mech. Behav. Biomed. Mater.* **2009**, *2*, 312.

34. Cao, Y. F.; Yang, D. H.; Soboyejoy, W. *J. Mater. Res.* **2005**, *20*, 2004.

35. Johnson, K. L. Contact Mechanics; Cambridge University Press: Cambridge, **1987**.

36. Sneddon, I. N. *Int. J. Eng. Sci.* **1965**, *3*, 47.

37. Kohna, J. C.; Ebenstein, D. M. *J. Mech. Behav.: Biomed. Mater.* **2013**, *20*, 316.

38. Nikolov, S.; Han, C.-S.; Raabe., D. *Int. J. Sol. Struct.* **2007**, *44*, 1582.

39. Han, C.-S.; Nikolov., S. *J. Mater. Res.* **2007**, *22*, 1662.

40. Tymiak, N. I.; Kramer, D. E.; Bahr, D. F.; Wyrobek, T. J.; Gerberich, W. W. *Acta Mater.* **2001**, *49*, 1021.

41. Gerberich, W. W.; Tymiak, N. I.; Grunlan, J. C.; Horstemeyer, M. F.; Baskes, M. I. *ASME J. Appl. Mech.* **2002**, *69*, 433.